Biophysical Chemistry 141 (2009) 75–86

Contents lists available at ScienceDirect

Biophysical Chemistry

journal homepage: http://www.elsevier.com/locate/biophyschem

Dynamic conformational changes due to the ATP hydrolysis in the motor domain of myosin: 10-ns molecular dynamics simulations

Tatsuyuki Kawakubo [a,*], Okimasa Okada [b], Tomoyuki Minami [c]

[a] Faculty of Engineering, Toin University of Yokohama, Aoba-ku, Yokohama 225-8502, Japan
[b] Medicinal Chemistry Laboratory, Mitsubishi Tanabe Pharma Corporation, Aoba-ku, Yokohama 227-0033, Japan
[c] Life Science Products Div., FUJIFILM Corporation, Minato-ku, Tokyo 106-8620, Japan

ARTICLE INFO

Article history:
Received 1 October 2008
Received in revised form 24 December 2008
Accepted 24 December 2008
Available online 13 January 2009

Keywords:
Molecular dynamics (MD) simulations
Myosin motor domain
ATP hydrolysis
Intramolecular motions of atoms
Dynamic structural fluctuations

ABSTRACT

Muscle contraction is caused by directed movement of myosin heads along actin filaments. This movement is triggered by ATP hydrolysis, which occurs within the motor domain of myosin. The mechanism for this intramolecular process remains unknown owing to a lack of ways to observe the detailed motions of each atom in the myosin molecule. We carried out 10-ns all-atom molecular dynamics simulations to investigate the types of dynamic conformational changes produced in the motor domain by the energy released from ATP hydrolysis. The results revealed that the thermal fluctuations modulated by perturbation of ATP hydrolysis are biased in one direction that is relevant to directed movement of the myosin head along the actin filament.

1. Introduction

Muscle contraction is caused by movement of myosin heads along actin filaments. The movement is driven by cyclic interactions between myosin and actin molecules caused by ATP hydrolysis, which occurs in the nucleotide active pocket within the myosin motor domain. For the process of cyclic myosin–actin interactions, several intermediate states and conformational changes have been presented on the basis of X-ray structure analyses [1–6], cryo-electron-microscopy [7], electron paramagnetic resonance (EPR) spectra [8], and mutational studies [9] of myosin heads complexed with nucleotide analogues. The following model for the cyclic process has been argued: association of ATP molecule with the myosin head, weakening of the myosin–actin binding, hydrolysis of ATP, release of ATP hydrolysis products through the back door of the myosin head, conformational changes in the motor domain including the junction between the lever arm and the myosin head, creation of the power stroke and a return to strong myosin–actin binding. Of these steps, bending of the junction between the lever arm and the head induced by ATP hydrolysis [2,3,5] is crucial for global movement of myosin along actin filament, but its mechanism still remains unknown. Furthermore, a kind of reversely-directed myosin motor, called myosin VI, is reported [10] and what determines the direction of movement of the myosin motor is of great importance.

On the other hand, single molecule observations by means of fluorescence microscopy revealed that the movement of the myosin head relative to the actin filament following hydrolysis of a single ATP consists of multiple random steps that are not always in the forward direction [11,12]. Furthermore, simultaneous measurements of the nucleotide release and the mechanical reaction of the myosin head showed that the reaction was not directly coupled with the nucleotide release [13].

To fully understand how a small chemical trigger at the nucleotide active site induces the mechanical reaction, it is desirable to examine the intramolecular processes following ATP hydrolysis in the myosin head. At present, however, there are no experimental means for observing the dynamic behaviors of each atom in a molecule. Molecular dynamics (MD) simulations provide us with information regarding both the static stability and the dynamic flexibility of subdomain conformations of a protein. In recent years, several MD simulations of myosin heads have been performed and are becoming complementary to experimental studies. Higo et al. [14] derived collective modes for subfragment-1 S1 of chicken skeletal myosin from MD trajectories of a backbone model and found large flipping motions of the α-helical C-terminal tail of S1 as the first and second largest amplitude collective modes, which are perpendicular to each other. Minehardt et al. [15] examined the molecular mechanism of ATP hydrolysis in the nucleotide-binding pocket by means of classical molecular mechanics (MM) simulations and quantum mechanical (QM) structural relaxations, and investigated the extent to which the P-loop, Switch I, and Switch II are involved in hydrolysis. MD simulations performed by Lawson et al. [16] revealed that relaxation

* Corresponding author.
E-mail address: tatsu@cc.toin.ac.jp (T. Kawakubo).

0301-4622/$ – see front matter © 2009 Elsevier B.V. All rights reserved.
doi:10.1016/j.bpc.2008.12.014

of ADP and free Pi from their initial position reduced the diameter of the back door via motion of Switch I and Switch II located in the upper and lower 50-kDa subdomains, respectively. Li and Cui [17] analyzed the functional motions of myosin using the block normal approach method and suggested that the collective displacement mainly concerns the converter region, whereas the local rearrangement involves the salt-bridge region between Switch I and Switch II. Zheng and Doniach [18] carried out normal mode analyses of the deviations of all Cα atomic coordinates induced by a local displacement of atoms in the nucleotide-binding pocket using an elastic network model and revealed that the displacements of atoms for myosin and F1-ATPase could be expressed in terms of one or two dominant lowest-frequency modes and their amplitudes were in good agreement with the measured ones. Navizet et al. [19] calculated B-factors as functions of the residue number for three conformations (near-rigor, detached and transition states) of the myosin head, containing the motor domain and the lever arm, with a coarse-grained elastic network model; and their results identified rigid and flexible domains within the myosin structure and highlighted the respective roles of the light chains and nucleotide binding. Takagi and Kikuchi [20] investigated the structural relaxation of the myosin motor domain from the pre-power stroke state to the near-rigor state in connection with the nucleotide release using MD simulations of a coarse-grained Go-like model and found that the myosin motor does not relax to the near-rigor conformation before the nucleotide dissociates. Koppole et al. [21] carried out MD simulations of *Dictyostelium discoideum* Myosin II motor crystallized with various ATP analogues and revealed that residue Asn475 in the Relay helix was pushed away from Switch II upon ATP hydrolysis and this sensing allowed the power stroke to start upon initial binding to actin. Liu et al. [22] performed an MD study of detailed residue-wise interactions involved in the binding of myosin to actin in the absence of nucleotide using the crystal structure of chicken skeletal myosin. They found that the 50-kDa/20-kDa loop (Loop 2) is in a conformation stabilized with internal salt bridges, and further revealed that the Cardiomyopathy loop forms interprotein salt bridges with actin monomers, whereas its Arg 405 residue, the mutation site associated with the hypertrophic Cardiomyopathy, forms an internal strong double salt bridges with Glu 605 of S1. In a previous paper [23], we examined how the energy released by ATP hydrolysis at the nucleotide-binding site expands throughout the motor domain, using 1-ns all-atom MD simulations of the myosin head at 300 K and found that intramolecular collective modes were stimulated at the actin-binding site and the junction with the neck. However, the run time of 1-ns was too short compared with the experimental time resolution. In the present study, we extended the run time of MD simulations to 10 ns and examined how ATP hydrolysis gives rise to dynamic conformational changes including fluctuations in the overall myosin motor domain.

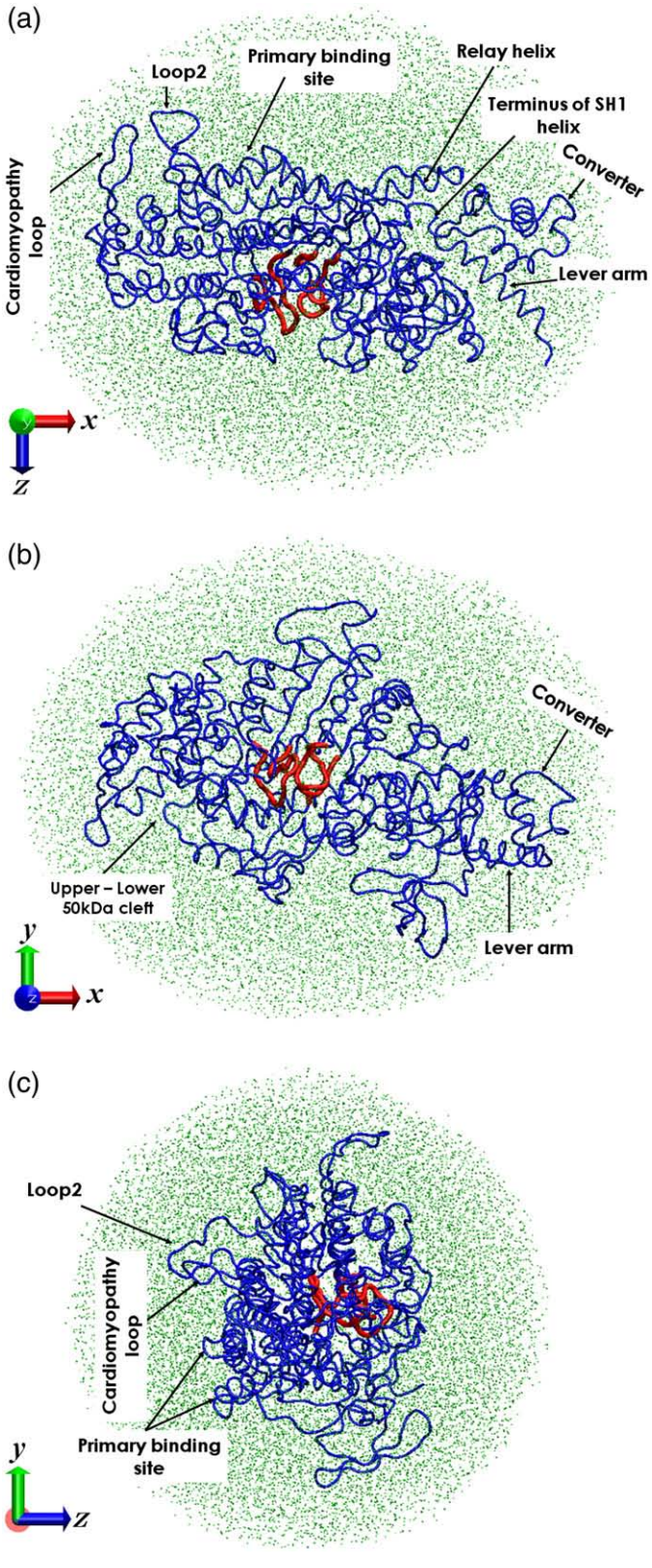

Fig. 1. Top (a), side (b) and front (from the actin side) (c) views of the backbone structure of the motor domain of myosin solvated with a spheroidal water droplet speckled in green. The ATP hydrolysis energy is distributed to the nucleotide-binding site shown in red. The conventional names of several parts of the myosin motor are included for convenience. The Cardiomyopathy loop, Loop 2 and Primary binding site are regions that directly interact with actin molecules. The converter and the lever arm constitute a tail, which links to the myosin filament. The upper–lower 50-kDa cleft is the exit for ATP hydrolysis products. The Relay helix is a signal transmission path from the nucleotide active site to the Primary binding site on one side and to the converter through the SH1 helix on the other side. It is noticeable that a terminus of the SH1 helix, which appears as a curved loop in the top view, is located between the head and the tail of the motor domain and seems to be a hinge joint connecting them.

2. Methods

The initial process in the MD simulations was the same as that in our previous study using a run time of 1 ns [23]. We truncated the motor domain (N-terminal 785 residues) from the structural data for nucleotide-free subfragment-1 S1 of scallop myosin (PDB; 1kk7, M. Himmel et al.) and added 34 missing residues (1–4, 23–25, 204, 211, 212, 365, 366, 406, 407, 451, 628–642 and 730–733) in the original data using the similar method explained by Lawson et al. [16] as follows. We built the missing parts by linking one resolved residue to the other resolved one with the missing residues using the Monte Carlo method. In this process the position of the alpha carbon atoms of the missing residues

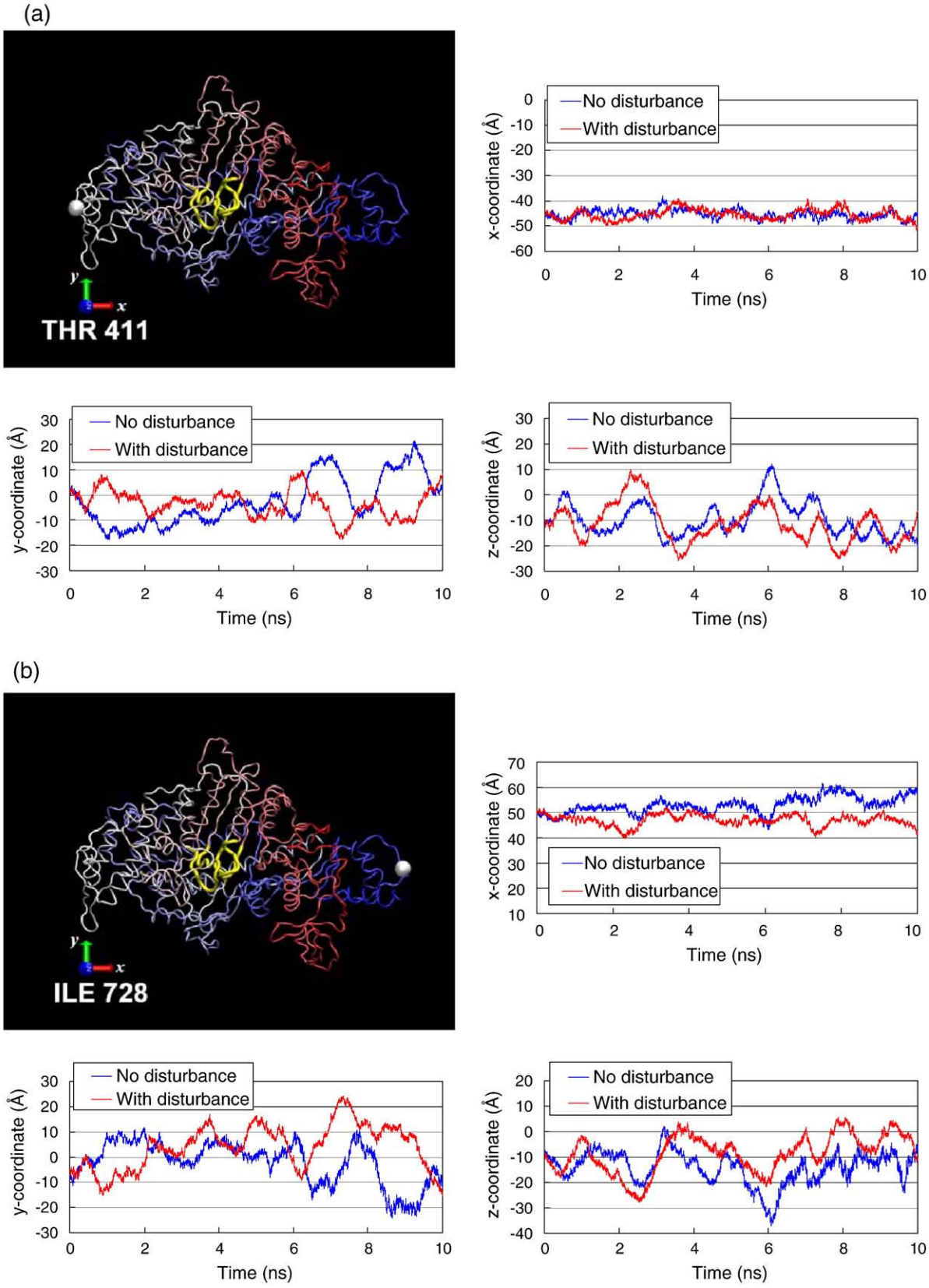

Fig. 2. The *x*, *y* and *z* components of the trajectories for α-carbons in six residues computed under two initial conditions, namely in the presence (red line) and absence (blue line) of a disturbance corresponding to ATP hydrolysis. The white sphere in the top-left structural map of each figure represents the position of the α-carbon in the relevant residue. The colors of the strings range from red to blue corresponding to increasing residue numbers. The nucleotide-binding sites are represented by bold yellow strings. The origin of the coordinates used in the trajectory graphs is taken at the center of the spheroidal water droplet shown in Fig. 1 and it corresponds to the center of the structural map. The directions of the *x*, *y* and *z* coordinates are defined as indicated by the red, green and blue arrows, respectively. The first three figures (a), (b) and (c) are concerned with residues located on the outskirts of the motor domain and their structural maps are side views from the (+*z*) direction, while the latter three figures (d), (e) and (f) are concerned with residues located at the junction between the head and the tail and their structural maps are side views from the (−*z*) direction. (a) Residue 411 is located in the region facing actin molecules. (b) Residue 728 is located in the converter linking to the lever arm. (c) Residue 633 is in the Loop 2 interacting with actin monomers. Residues 507 (d), 708 (e) and 765 (f) differ in their position number, but are spatially in close proximity, thereby leading to similar trajectories.

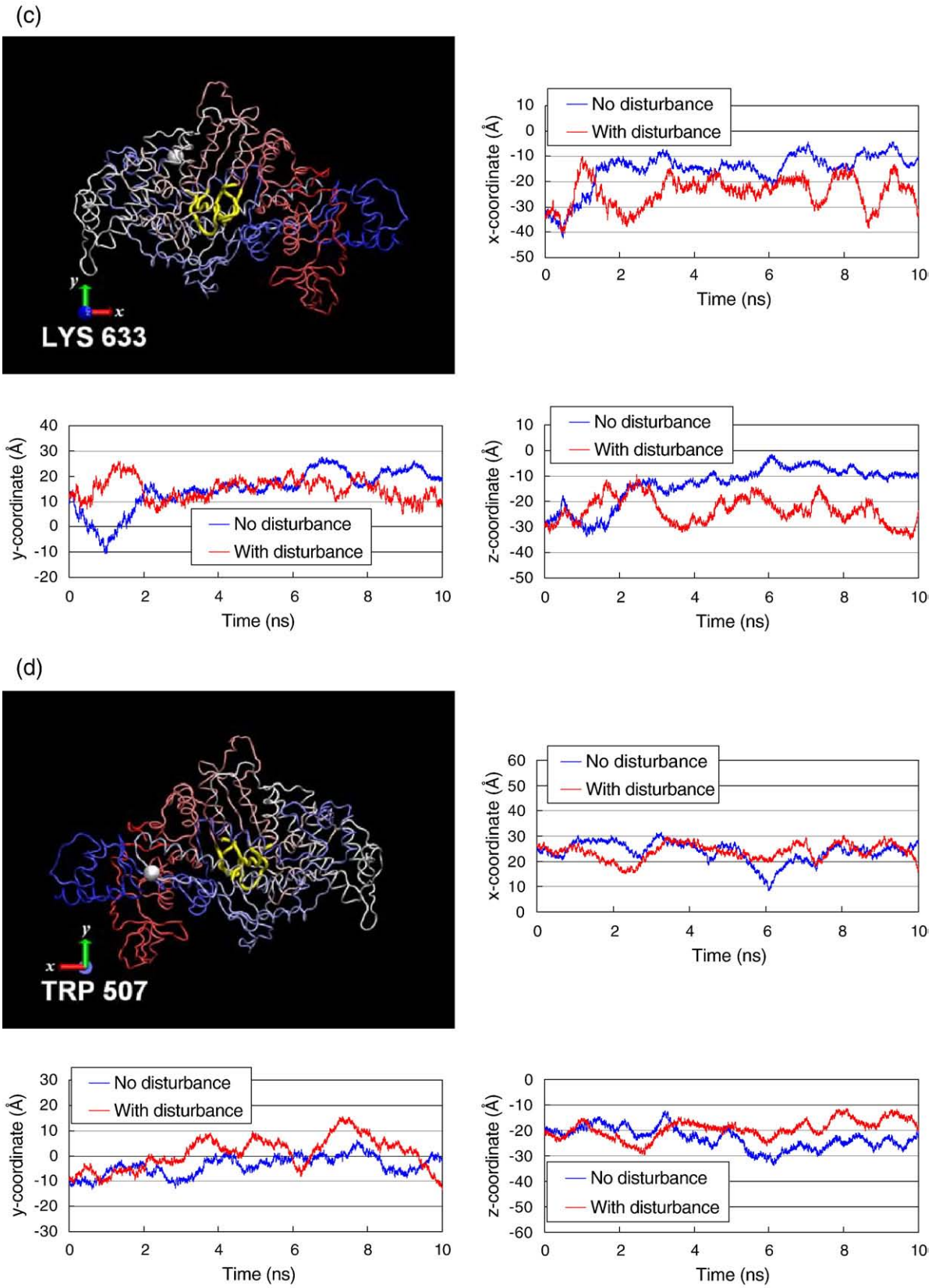

Fig. 2 (*continued*).

were first determined and the rest of atoms were added by LEaP module in AMBER 8 [24]. The built parts were energy minimized and then solvated in a cap water droplet separately to be equilibrated using MD calculation at 300K for 1 ns, where the repaired atoms and water molecules were allowed to move. After this repairing, the motor domain was solvated with a spheroidal water droplet as shown in Fig. 1. The soft half-harmonic potential [24] was applied to prevent the water molecules from evaporating. The whole system comprising polypeptides and water

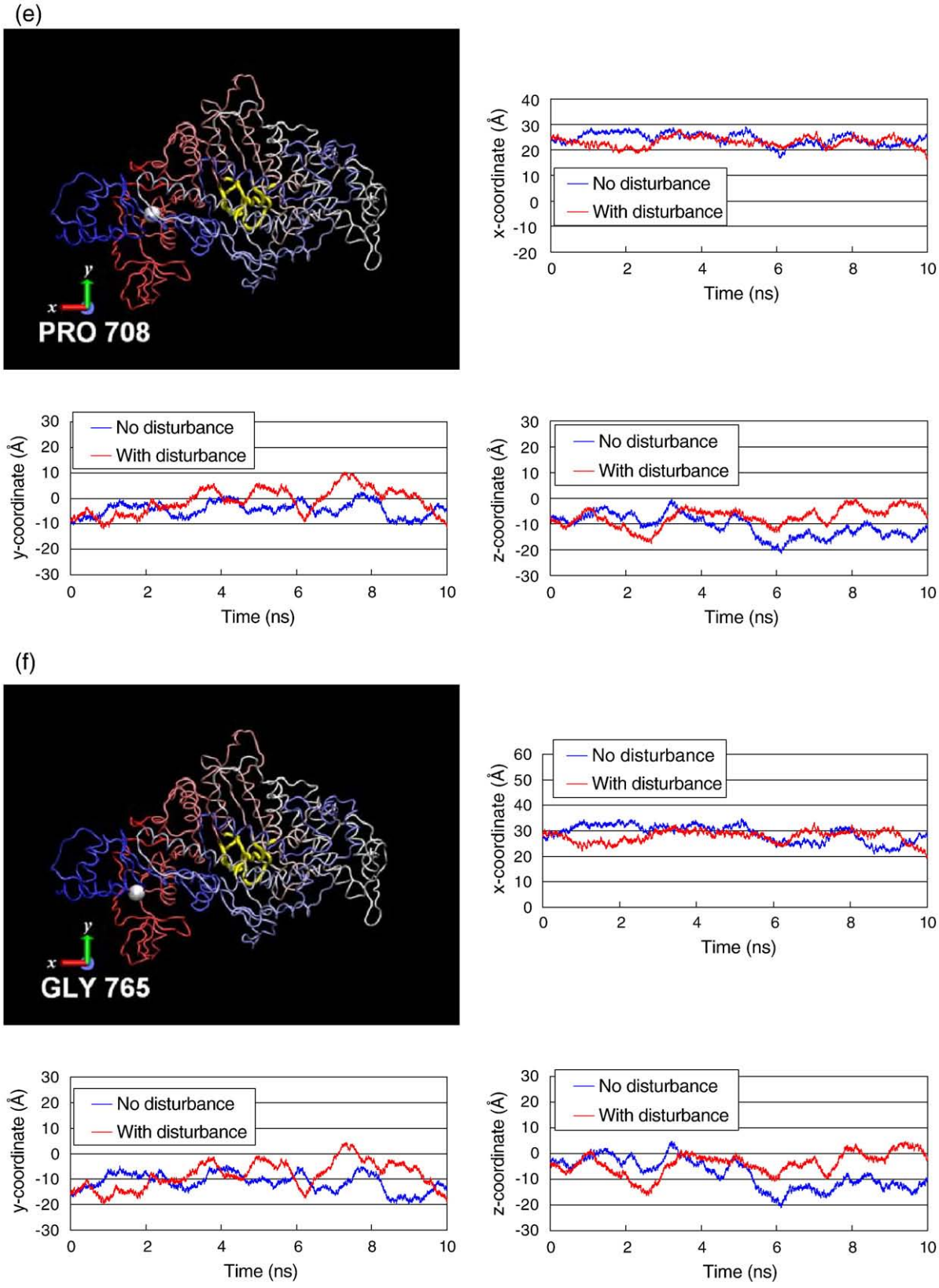

Fig. 2 (*continued*).

molecules was thermally equilibrated at 300 K for 300 ps. The total number of atoms was 68,662 and that of water molecules was 18,727. After this process, the trajectories of each atom were calculated under the following two initial conditions.

1. Without giving any disturbance to the whole system, we continued to calculate the trajectories for 10 ns. The temperature defined by the average of kinetic energy of the atoms was left uncontrolled.

2. An energy of 8.60×10^{-20} J released by hydrolysis of one ATP molecule was distributed to 80 backbone atoms as kinetic energy by giving an additional velocity to each atom in proportion to its instantaneous velocity after the equilibration run without changing its direction so as to give an impact that was as small as possible. The atoms supplied with energy were located within a 10-Å radius (shown in red in Fig. 1) around the position that the γ-phosphate would occupy when a nucleotide was associated with the myosin head. The reason why we chose the radius of 10 Å is that the residues within this sphere can be in direct contact with the γ-phosphate. Among the 80 atoms, 29 belonged to the P-loop, 40 to Switch I and 11 to Switch II and those atoms correspond to the residues ascertained by MM simulations to form hydrogen bonding to the γ-phosphate in *D. discoideum* myosin [15]. After giving the disturbance, MD calculations were carried out for 10 ns with the temperature left uncontrolled.

The calculations were carried out using a computer loaded with a special purpose chip MDGRAPE-3 (High-Performance Molecular Simulation Team, RIKEN, Tsurumi, Yokohama, Japan) that enabled us to calculate the electrostatic and van der Waals interactions of every atomic pair without using the cut-off method. The software was the SANDER module in AMBER 8. We used the AMBER force field with parm96 parameters [25] and the TIP3P model [26] for explicit water molecules. A time step of 2 fs was used with the SHAKE algorithm [27]. Berendsen's method [28] was used for temperature regulation during the initial thermal equilibration, but the temperature was not regulated during the sampling runs with different initial conditions. The final temperature at 10 ns obtained from the average kinetic energy of all atoms during the last 100 ps was 310 K in both the absence and presence of disturbance. A deviation of 10 K from 300 K was encountered due to an accumulation of computational errors. The graphical representations were prepared with VMD [29] and ViewerLite (Accelrys Inc., San Diego, CA, USA).

3. Results of simulations

3.1. Trajectories of α-carbons in representative residues with and without initial disturbance

Fig. 2 shows the positions of α-carbons in six residues and their *x*, *y* and *z* components of their trajectories for 10 ns under two different initial conditions. The blue line in each graph represents the trajectories in the absence of disturbance and the red line represents those in the presence of disturbance that was initially given to 80 atoms around the ATPase pocket. The origin of the *x*, *y* and *z* coordinates was taken at the center of the spheroidal water droplet in Fig. 1, and the *x* axis was defined in the horizontal direction, with the *y* axis in the vertical direction and the *z* axis perpendicular to the *x*–*y* plane.

In Fig. 2(a), the trajectories of residue Thr411, which is located at the Cardiomyopathy loop that would be in contact with actin monomers in the presence of actin filament, largely fluctuate in the *y* and *z* coordinates

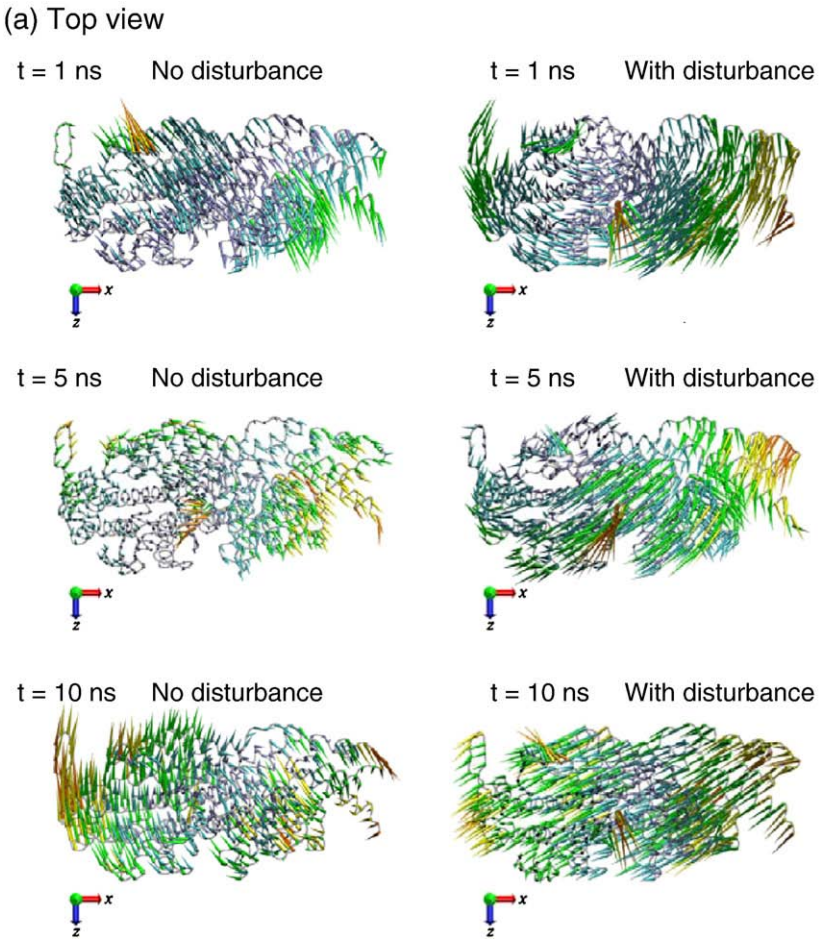

Fig. 3. Top (a), side (b) and front (c) views of the shifts of each α-carbon atom at 1 ns, 5 ns and 10 ns from its 10-ns average position of *undisturbed thermal fluctuations*, which is indicated by the blue string. The "without disturbance" case is shown in the left column and the "with disturbance" case is shown in the right column in each figure. The colors of the cones indicate the magnitude of the deviation changing from blue (small) to orange (large).

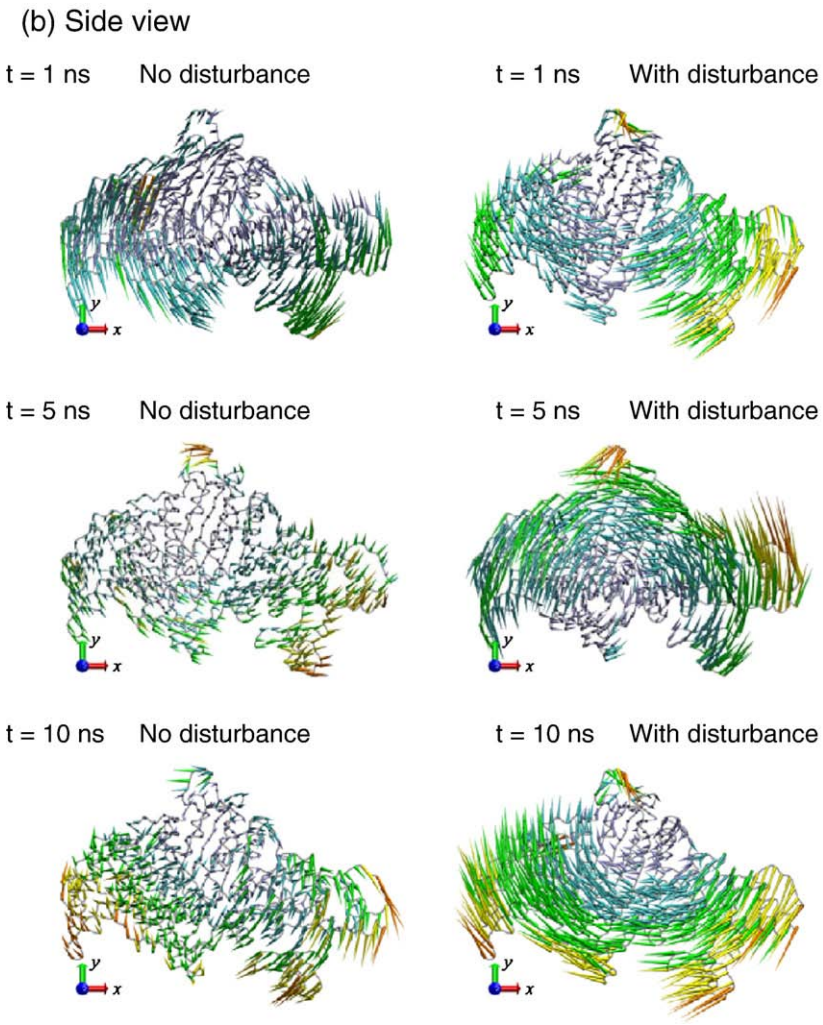

Fig. 3 (*continued*).

compared with those in the *x* coordinate, in both the presence (red) and absence (blue) of disturbance. The same kinds of large fluctuations in the *y* and *z* coordinates are found for residue Ile728, which is located at the converter linking to the lever arm (Fig. 2(b)). Meanwhile, the red and blue trajectories for residue Lys633 in the Loop 2, which is considered to form a stable binding with actin monomers [9,22], steadily deviate from each other in the *x* and *z* coordinates (Fig. 2(c)).

Since residue 728 is 55 Å away from the ATPase pocket (central yellow strings), the issue of how the ATP hydrolysis signal can be transmitted from the nucleotide-binding site to the converter or the lever arm is of great interest. Fig. 2(d), (e) and (f) represent the trajectories of residues of Trp507, Pro708 and Gly765, respectively. The structural maps on the top-left in these figures are side views from (−*z*) direction. Residue 507 is located at a terminus of the Relay helix connected with Switch II, residue 708 is at a joint between the SH1 helix and the converter, and residue 765 is at a junction between the converter and the lever arm. Although these residues are rather different in their position numbers, they are spatially in close proximity and can interact with each other, thereby leading to fairly similar trajectories. Furthermore, we can see that their deviational behaviors of the red lines from the blue ones in the *y* and *z* coordinates are emphasized for trajectories of residue 728 at the converter observed in Fig. 2(b). This indicates that the ATP hydrolysis signal can be transmitted to the lever arm from Switch II through these bypasses.

In the general views presented in Fig. 2, the red and blue trajectories appear to be the same kinds of thermal fluctuations, but we inferred that the red trajectories may involve some behaviors that the blue trajectories do not, and produce some effects on the motor domain as a global output. Thus, we referred to the red trajectories subject to ATP hydrolysis as *modulated thermal fluctuations* and referred to the blue trajectories in the absence of disturbance as *undisturbed thermal fluctuations*. The top-left image in each figure is a 10-ns average conformation of the *undisturbed thermal fluctuations*.

3.2. Shifts of each α-carbon atom from its thermal average position at three moments

Fig. 3 shows the positions of each α-carbon atom at 1-ns, 5-ns and 10-ns shifting from its 10-ns average position in the *undisturbed thermal fluctuations*. Since the structure of a protein always varies subject to thermal fluctuations at the molecular level, at the molecular level, we have defined here the 10-ns *undisturbed thermal average structure* as the standard conformation of the motor domain at 300 K. Each atomic shift from its standard position in the absence of disturbance is shown in the left column and that in the presence of disturbance is shown in the right column. In the *x*–*z* projection diagrams of the top views in Fig. 3(a), the fluctuations have a tendency to shift rotationally in one direction, while in the *x*–*y* projection diagrams of the side views in Fig. 3(b), clockwise and counterclockwise rotational modes appear alternately. The front views from the (−*x*) direction in Fig. 3(c) show the

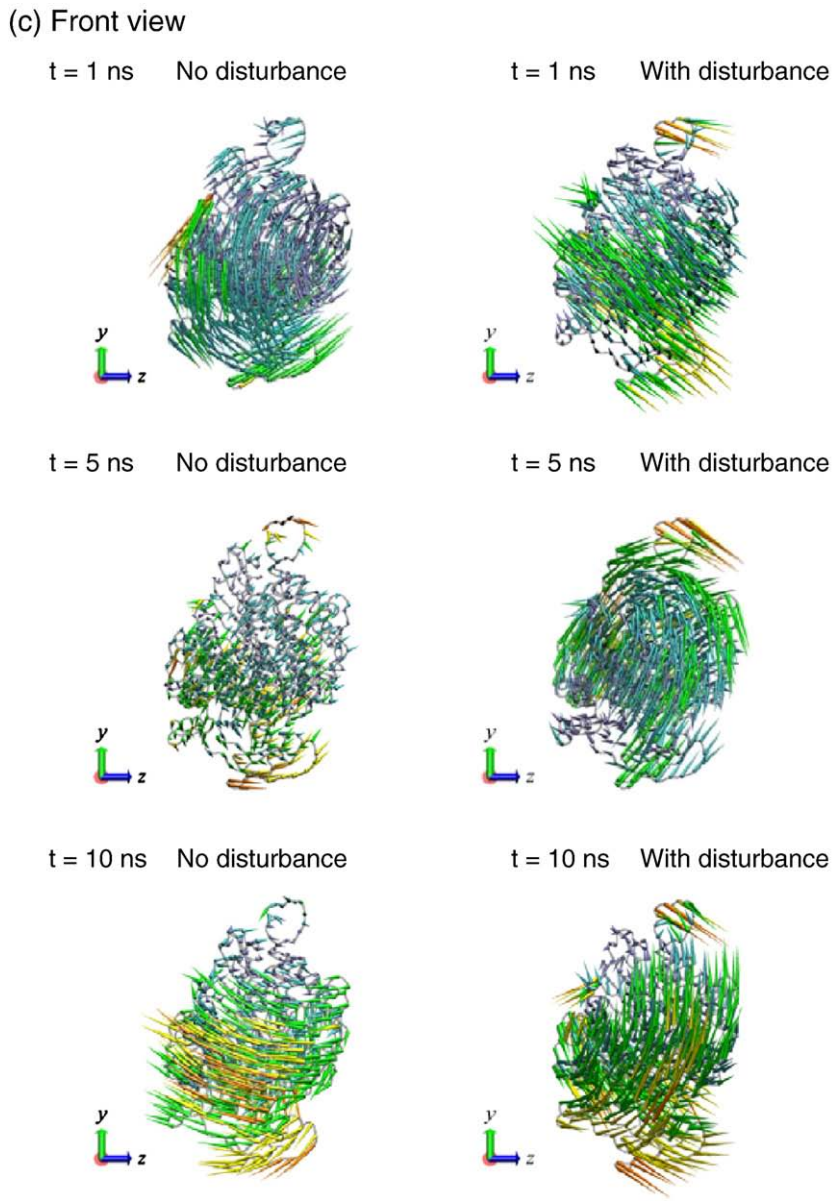

Fig. 3 (*continued*).

y–*z* projection diagrams of atomic shifts corresponding to those in Fig. 3(a) and (b).

3.3. Root mean squares of deviations

To examine the behaviors of the fluctuations of each atom subject to ATP hydrolysis, three kinds of root mean squares of fluctuations (*RMS*) were considered. The first root mean square, *RMS*1, is that of deviations of the *undisturbed thermal fluctuations* from their average positions, and the second root mean square, *RMS*2, is that of deviations of the *modulated fluctuations* from their average positions. To clarify the effect of the disturbance, we calculated another root mean square, *RMS*3, which represents the root mean square of deviations of the *modulated fluctuations* from the average positions of the *undisturbed thermal fluctuations*. *RMS*3 reflects the magnitude of fluctuations including static conformational changes from the undisturbed structure, while *RMS*2 represents the deviations of modulated fluctuations from their average. If we denote the coordinates of an α-carbon in the presence of ATP hydrolysis by (*x*, *y*, *z*) (*undisturbed thermal fluctuation coordinates*) and those in the absence of ATP hydrolysis by (*X*, *Y*, *Z*) (*modulated thermal fluctuation coordinates*), *RMS*1, *RMS*2 and *RMS*3 are expressed by the following equations:

$$RMS1 = \sqrt{< (x - < x >)^2 + (y - < y >)^2 + (z - < z >)^2 >} \quad (1)$$

$$RMS2 = \sqrt{< (X - < X >)^2 + (Y - < Y >)^2 + (Z - < Z >)^2 >} \quad (2)$$

$$RMS3 = \sqrt{< (X - < x >)^2 + (Y - < y >)^2 + (Z - < z >)^2 >}, \quad (3)$$

where <···> is the time average over 10 ns.

Fig. 4(a) shows a comparison of *RMS*1 (blue curve) with *RMS*2 (red curve). The three red rectangles denote the residues within the P-loop, Switch I and Switch II to which the ATP hydrolysis energy is distributed. The red and blue curves have roughly the same dependence on the residue number, meaning that the magnitudes of the fluctuations are qualitatively the same in the presence and

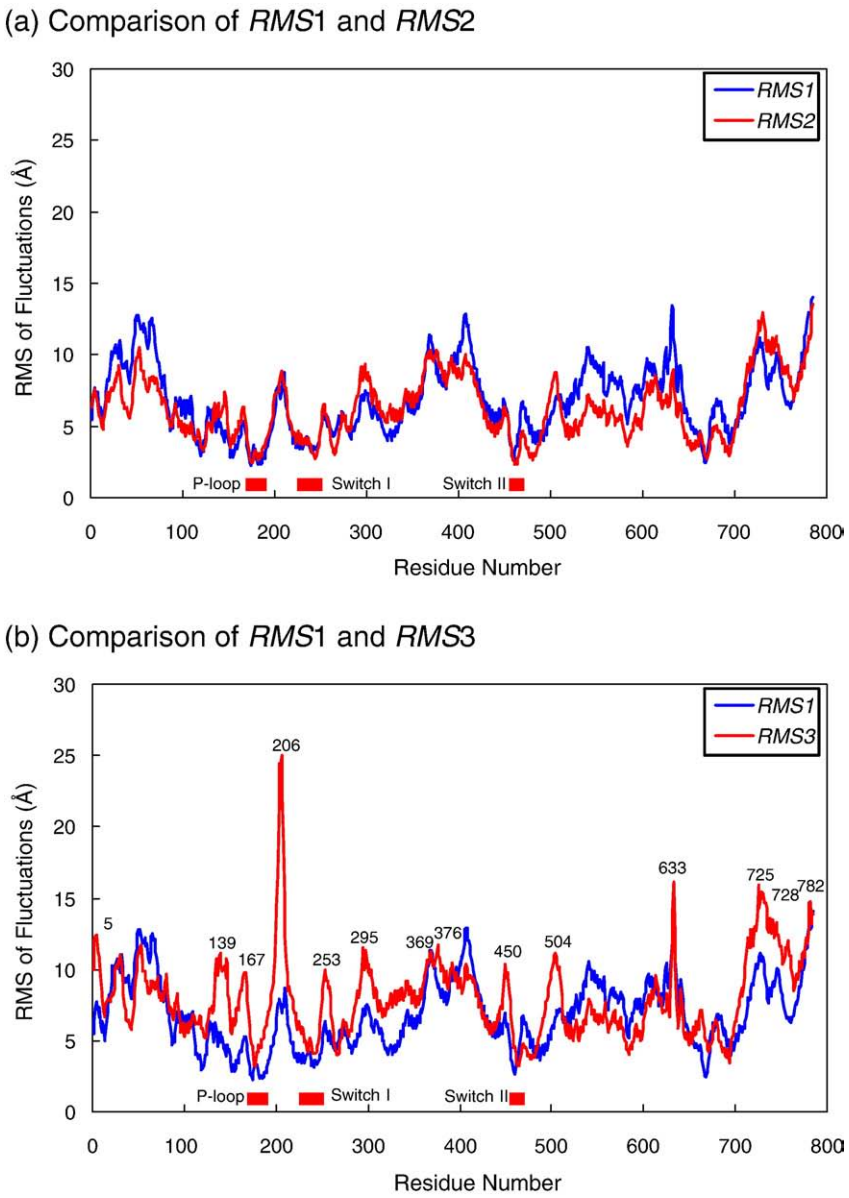

Fig. 4. Root mean squares of deviations (*RMS*) of atomic positional fluctuations versus residue number. (a) Comparison of *RMS*1 and *RMS*2 defined by Eqs. (1) and (2), respectively. (b) Comparison of *RMS*1 and *RMS*3 defined by Eqs. (1) and (3), respectively. The three red rectangles denote residues within the P-loop, Switch I and Switch II to which the ATP hydrolysis energy is distributed.

absence of disturbance. Fig. 4(b) shows a comparison of *RMS*1 (blue curve) and *RMS*3 (red curve), where the *RMS*3 reflects the dynamic conformational changes due to ATP hydrolysis from the thermal equilibrium structure. The red and blue curves also have similar dependences in this comparison, which is known as *the general relationship between fluctuations and response to a stimulus* [30,31]. However, the responses are fairly enhanced at several residues located in the so-called *loops* on the outskirts of the motor domain. Particularly, residue 206 exhibits an extraordinarily large peak due to superposed effects from disturbances given at the P-loop and Switch I, and residues 167, 253 and 450 are also directly affected by disturbances at the P-loop, Switch I and Switch II, respectively. Furthermore, enhancements of *RMS*3 are seen at the following sites; residue 504 near the terminus of the Relay helix, which connects Switch II with the Primary binding site facing the actin monomers, residue 633 in Loop 2, which is the junction between the 50-kDa and 20-kDa subdomains and provides highly charged contacts to an actin monomer [22], and residues 715–764 at the converter linking to the lever arm. Thus, the results of our 10-ns MD simulations can be described as follows: a small local disturbance due to ATP hydrolysis seems to induce dynamic conformational changes at several sites in the motor domain, which exceed undisturbed thermal fluctuations.

3.4. 10-ns average structures with and without initial disturbance superimposed at the junction with the lever arm

The actual myosin head is linked to the fixed myosin filament via a long lever arm wrapped in the essential and regulatory light chains, so that changes in the orientation of the head will be amplified. Although our simulations are confined to the motor domain, we tried to superimpose 10-ns average structures with and without disturbance at the junction with the lever arm (residues 761–775). Fig. 5 shows superimposed 10-ns average structures of *modulated thermal fluctuations* (red) and *undisturbed thermal fluctuations* (white) represented by ribbon diagram. The *loops* on the outskirts of the myosin head are flexible and therefore strongly transformed (from white to red) by the disturbance caused by ATP hydrolysis. The *α-helices* are also seen to shift at several sites because they are connected with the *loops*. In Fig. 5

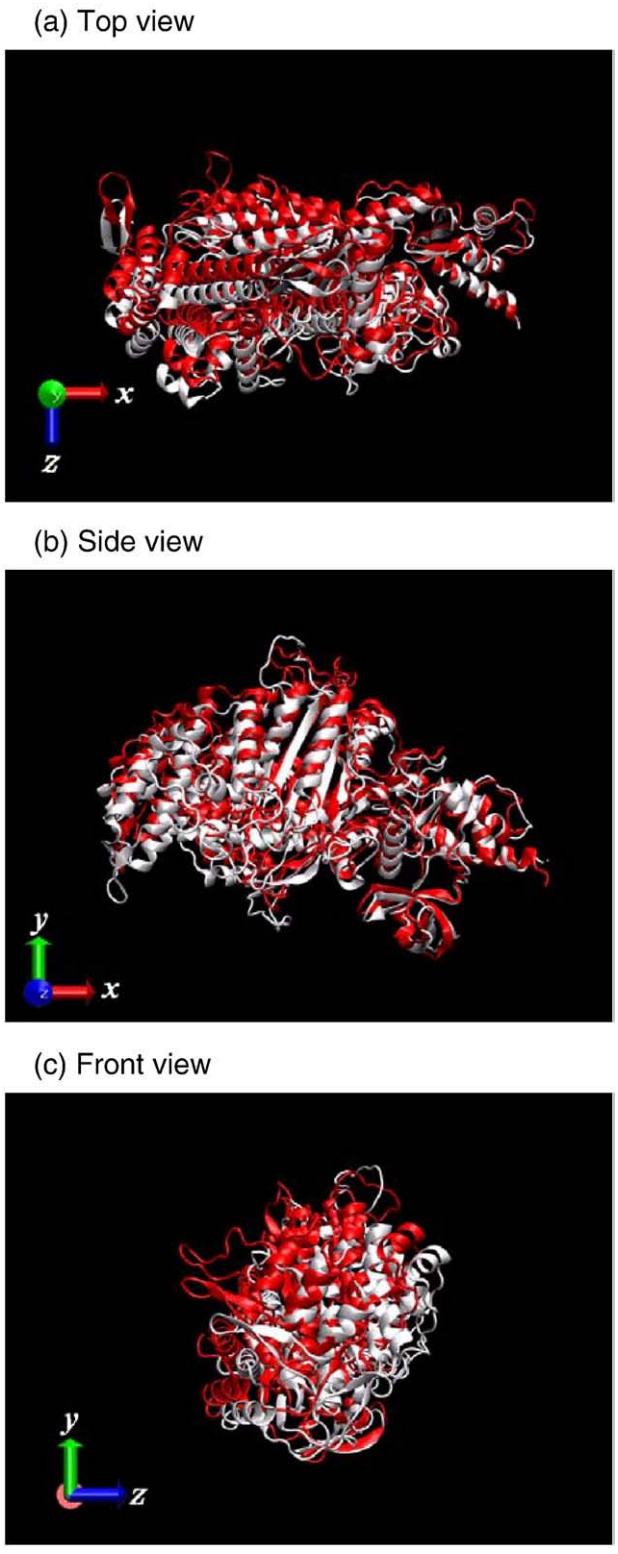

Fig. 5. Top (a), side (b) and front (c) views of 10-ns average structures with (red) and without (white) disturbance superimposed at the junction with the lever arm (residues 761–775). Deviations from the white structure to the red structure represent conformational changes caused by the ATP hydrolysis.

(a), we can see that the head of the motor domain globally makes a clockwise rotations in the x–z plane around a hinge joint at the terminus (Phe707, Pro708) of the SH1 helix (see Fig. 1(a)), which is connected to the converter. A rather small clockwise rotation in the x–y plane around the same hinge joint is also found in Fig. 5(b). In Fig. 5(c) which is a view from actin side, we can see that averaged positions of the actin-binding sites such as the Cardiomyopathy loop, Loop 2 and Primary binding site shift to the $(+y, -z)$ direction in the presence of disturbance due to ATP hydrolysis.

3.5. Dynamic structural fluctuations superimposed on the initial position of the junction with the lever arm

To visualize the dynamic conformational changes due to ATP hydrolysis, we superimposed fluctuating structures in the absence and presence of disturbance every 1 ns from 0 to 10 ns on the initial (t=0 ns) positions of the junction with the lever arm. Fig. 6(a) shows the top views (from the $(+y)$ direction) of the dynamic structures, in which the range of fluctuations is seen to widen in the $(-z)$ direction in the presence of disturbance so as to give a clockwise rotational biasing of the motor domain hinged on a joint around residues Phe707 and Pro708 at the terminus of the SH1 helix linking to the converter. The black line denotes the initial structure at t=0 ns. In the side views (from the $(+z)$ direction) of the dynamic structures shown in Fig. 6(b), the range of fluctuations is not as large in both the presence and absence of disturbance. In Fig. 6(c), which shows the front views from the actin filament side, the range of fluctuations of the actin-binding site is found to shift to the $(+y, -z)$ direction so as to twist the myosin head along the x axis in the presence of disturbance. These biased fluctuations of the motor domain may produce a unidirectional interaction with the actin monomers.

4. Discussion

The effect of disturbance due to ATP hydrolysis in the nucleotide-binding pocket was found to spread throughout the myosin head in 2 ns at longest in the form of modulation of thermal fluctuations (Fig. 2). The modulation signal is transmitted not only along the main chain of backbone atoms but also through bypasses between residues of non-sequential numbers, for instance Trp 507, Pro 708 and Gly 765, which are spatially in close proximity (Fig. 2(d), (e) and (f)) in the protein folding structure and show fairly similar trajectories. The same kind of trajectory similarity was observed between Gly463 in Switch II and Asn481 in Relay helix (not shown in Fig. 2), which corresponds to the coupling between Switch II and Asn475 in Relay helix previously reported for *D. discoideum* [21]. Thus the signal from the nucleotide active site is transmitted through these bypasses to the tail part of myosin and induces large swinging deviations of the converter and the lever arm from their average positions in the *undisturbed thermal equilibrium state*. Their deviations in the x–z projection have a tendency of unidirectional shift (Fig. 3(a)), while those in the x–y projection show alternating shift with clockwise and counterclockwise rotations (Fig. 3(b)).

These deviations of residues from thermal equilibrium positions are reflected in the difference between *RMS*3 (red) and *RMS*1 (blue) curves in Fig. 4(b). *RMS*3 represents the magnitude of fluctuations of the residue's positions including static conformational changes from the undisturbed structure and it is fairly enhanced at several sites. Its residue number dependence qualitatively agrees with the amplitude of the computed displacement induced by the nucleotide pocket deformation from ADP-BeFx state (PDB ID code 1kk8) to the nucleotide free state (PDB ID code 1kk7) [18] and also with the calculated B-factor for structures of ADP.VO_4 (PDB ID code 1DFL) [19]. Out of enhanced sites, residue 504 is located near the terminus of the Relay helix that is a signal transmission path from nucleotide active site to the converter through the bypass 507/708 mentioned above, residue 633 is in Loop 2 that is very flexible and was reported to provide highly charged contacts to an actin monomer [22] and residues 715–764 constitute the converter linking to the lever arm. *RMS*3 at the Cardiomyopathy loop (404–418) and the Primary binding

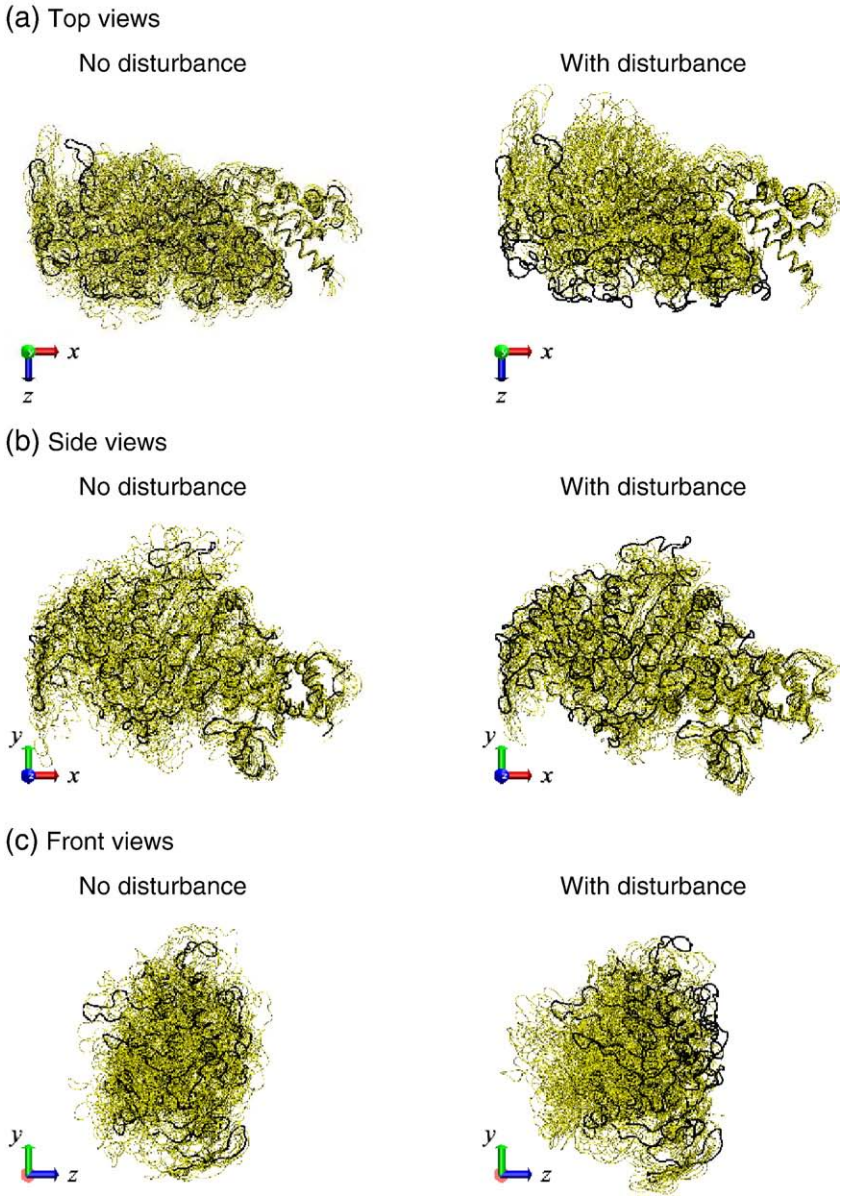

Fig. 6. Top (a), side (b) and front (c) views of fluctuating structures at every 1 ns from 0 to 10 ns superimposed on the initial (0-ns) position of the junction with the lever arm. The "without disturbance" case is represented in the left column and the "with disturbance" case is represented in the right column in each figure. The black line denotes the initial structure at $t=0$ ns.

site (529–562), both of which contact with actin molecules in the rigor state [22], is not so large compared with *RMS*1.

In an actual myosin molecule, however, another end of the lever arm is fixed with the myosin filament, so that swinging motions of the converter and the lever arm will rebound upon motions of the whole myosin head. As shown in Fig. 5, which represents 10-ns average structures superimposed at the lever arm in the presence (red) and the absence (white) of disturbance, the head of the motor domain makes a global bending to the $(+y, -z)$ direction (from white to red) around a hinge joint at the junction between the head and the lever arm. Thus the conformational deviations are emphasized at the Cardiomyopathy loop and the Primary binding site in the superimposed diagram. These conformational changes are qualitatively consistent with the results of snapshots obtained from structural analyses of myosin heads complexed with nucleotide analogues [1–3,5–9].

However, the dynamic activities of the motor domain can hardly be elucidated only in terms of a sequence of transient conformations. A crucially important point is that each atom thermally vibrates [11–13] around a position of the new averaged conformation in the presence of ATP hydrolysis (red ribbon diagrams in Fig. 5), which is deviated from that in the ATP-free state (white ribbon diagrams in Fig. 5). In general, the energy landscape of a protein has multiple potential minima, and large scale fluctuations, which jump over their barriers, consist of several anisotropic collective modes [32]. The biased fluctuations of the actin-binding site shown in Fig. 6(a) and (c) are conceived to be a reflection of the anisotropic collective vibrations induced by the disturbance. The unidirectional biased fluctuations of the motor domain shown in Fig. 6 (a) and (c) may push away actin molecules at a certain probability and the rebounding force will give a recovery stroke to the myosin head. The disturbance produced by ATP hydrolysis is an internal force for the myosin molecule, so that it can generate a force externally only when the lever arm is fixed to a heavy filament. The behavior of the motor domain is stochastic but similar to that of a batting player, who stands firmly on the ground and hits a ball by a directed twist of the waist and a swing of the arms.

The myosin head was found to make biased swinging motions around a hinge at the junction with the lever arm when the lever arm was fixed. However, whether these biased fluctuations could

stochastically generate forces to push away actin molecules and what determines the directionality of relative movements [10] are subjects remaining to MD simulations in the future.

References

[1] I. Rayment, H.M. Holden, M. Whittaker, C.B. Yohn, M. Lorenz, K.C. Holmes, R.A. Milligan, Structure of the actin–myosin complex and its implications for muscle contraction, Science 261 (1993) 58–65.

[2] Y. Sugimoto, M. Tokunaga, Y. Takezawa, M. Ikebe, K. Wakabayashi, Conformational changes of the myosin heads during hydrolysis of ATP as analyzed by X-ray solution scattering, Biophys. J. 68 (1995) 29s–34s.

[3] A. Houdusse, V.N. Kalabokis, D. Himmel, A.G. Szent-Györgyi, C. Cohen, Atomic structure of scallop myosin subfragment S1 complexed with MgADP: a novel conformation of the myosin head, Cell 97 (1999) 459–470.

[4] C.B. Bauer, H.M. Holden, J.B. Thoden, R. Smith, I. Rayment, X-ray structures of the apo and MgATP-bound states of *Dictyostelium discoideum* myosin motor domain, J. Biol. Chem. 275 (2000) 38494–38499.

[5] D.M. Himmel, S. Gourinath, L. Reshetnikova, Y. Shen, A.Z. Szent-Györgyi, C. Cohen, Crystallographic findings on the internally uncoupled and near-rigor states of myosin: further insights into the mechanics of the motor, Proc. Natl. Acad. Sci. U. S. A. 99 (2002) 12645–12650.

[6] S. Fischer, B. Windshügel, D. Horak, K.C. Holmes, J.C. Smith, Structural mechanism of the recovery stroke in the myosin molecular motor, Proc. Natl. Acad. Sci. U. S. A. 102 (2005) 6873–6878.

[7] K.C. Holmes, I. Angert, F.J. Kull, W. Jahn, R.R. Schröder, Electron cryo-microscopy shows how strong binding of myosin to actin releases nucleotide, Nature 425 (2003) 423–427.

[8] N. Naber, T.J. Purcell, E. Pate, R. Cooke, Dynamics of the nucleotide pocket of myosin measured by spin-labeled nucleotides, Biophys. J. 92 (2007) 172–184.

[9] H. Onishi, M.F. Morales, A closer look at energy transduction in muscle, Proc. Natl. Acad. Sci. U. S. A. 104 (2007) 12714–12719.

[10] J. Ménétrey, A. Bahloul, A.L. Wells, C.M. Yengo, C.A. Morris, H.L. Sweeney, A. Houdusse, The structure of the myosin VI motor reveals the mechanism of directionality reversal, Nature 435 (2005) 779–785.

[11] T. Yanagida, S. Esaki, A.H. Iwane, Y. Inoue, A. Ishijima, K. Kitamura, H. Tanaka, M. Tokunaga, Single-motor mechanics and models of the myosin motor, Phil. Trans. R. Soc. Lond. B355 (2000) 441–447.

[12] K. Kitamura, M. Tokunaga, A.H. Iwane, T. Yanagida, A single myosin head moves along an actin filament with regular steps of 5.3 nanometres, Nature 397 (1999) 129–134.

[13] A. Ishijima, H. Kojima, T. Funatsu, M. Tokunaga, H. Higuchi, H. Tanaka, T. Yanagida, Simultaneous observation of individual ATPase and mechanical events by a single myosin molecule during interaction with actin, Cell 92 (1998) 161–171.

[14] J. Higo, Y. Sugimoto, K. Wakabayashi, H. Nakamura, Collective motions of myosin head derived from backbone molecular dynamics and combination with X-ray solution scattering data, J. Comput. Chem. 22 (2001) 1983–1994.

[15] T.J. Minehardt, N. Marzari, R. Cooke, E. Pate, P.A. Kollman, R. Car, A classical and ab initio study of the interaction of the myosin triphosphate binding domain with ATP, Biophys. J. 82 (2002) 660–675.

[16] J.D. Lawson, E. Pate, I. Rayment, R.G. Yount, Molecular dynamics analysis of structural factors influencing back door P_i release in myosin, Biophys. J. 86 (2004) 3794–3803.

[17] G. Li, Q. Cui, Analysis of functional motions in Brownian molecular machines with an efficient block normal mode approach: Myosin-II and Ca^{2+}-ATPase, Biophys. J. 86 (2004) 743–763.

[18] W. Zheng, S. Doniach, A comparative study of motor–protein motions by using a simple elastic-network model, Proc. Natl. Acad. Sci. USA 100 (2003) 13253–13258.

[19] I. Navizet, R. Lavery, R.L. Jernigan, Myosin flexibility: structural domains and collective vibrations, Proteins 54 (2004) 384–393.

[20] F. Takagi, M. Kikuchi, Structural change and nucleotide dissociation of myosin motor domain: dual Go model simulation, Biophys. J. 93 (2007) 3820–3827.

[21] S. Koppole, J.C. Smith, S. Fischer, Simulations of the myosin II motor reveal a nucleotide-state sensing element that controls the recovery stroke, J. Mol. Biol. 361 (2006) 604–616.

[22] Y. Liu, M. Scolari, W. Im, H.J. Woo, Protein–protein interactions in actin–myosin binding and structural effects of R405Q mutation: a molecular dynamics study, Proteins 64 (2006) 156–166.

[23] T. Kawakubo, O. Okada, T. Minami, Molecular dynamics simulations of evolved collective motions of atoms in the myosin motor domain upon perturbation of the ATPase pocket, Biophys. Chem. 115 (2005) 77–85.

[24] D.A. Case, T.A. Darden, T.E. Cheatham III, C.L. Simmerling, J. Wang, R.E. Duke, R. Luo, K.M. Merz, B. Wang, D.A. Pearlman, M. Crowley, S. Brozell, V. Tsui, H. Gohlke, J. Mongan, V. Hornak, G. Cui, P. Beroza, C. Schafmeister, J.W. Caldwell, W.S. Ross, P.A. Kollman, AMBER 8, University of California, San Francisco, 2004.

[25] W.D. Cornell, P. Cieplak, C.I. Bayly, I.R. Gould, K.M. Merz Jr., D.M. Ferguson, D.C. Spellmeyer, T. Fox, J.W. Caldwell, P.A. Kollman, A second generation force field for the simulation of proteins, nucleic acids, and organic molecules, J. Am. Chem. Soc. 117 (1995) 5179–5197.

[26] W.L. Jorgensen, J. Chandrasekhar, J. Madura, M.L. Klein, Comparison of simple potential functions for simulating liquid water, J. Chem. Phys. 79 (1983) 926–935.

[27] J.P. Ryckaert, G. Ciccotti, H.J.C. Berendsen, Numerical integration of the Cartesian equations of motion of a system with constraints: molecular dynamics of *n*-alkanes, J. Comput. Phys. 23 (1977) 327–341.

[28] H.J.C. Berendson, J.P.M. Postma, W.F. van Gunsteren, A. DiNola, J.R. Haak, Molecular dynamics with coupling to an external bath, J. Chem. Phys. 81 (1984) 3684–3690.

[29] W. Humphrey, A. Dalke, K. Schulten, VMD-visual molecular dynamics, J. Mol. Graph. 14 (1997) 33–38.

[30] K. Sato, Y. Ito, T. Yomo, K. Kaneko, On the relation between fluctuation and response in biological systems, Proc. Natl. Acad. Sci. U. S. A. 100 (2003) 14086–14090.

[31] M. Ikegami, J. Ueno, M. Sato, A. Kidera, Protein structural change upon ligand binding: linear response theory, Phys. Rev. Lett. 94 (078102) (2005) 1–4.

[32] A. Kitao, S. Hayward, N. Go, Energy landscape of a native protein: jumping-among-minima model, Proteins 33 (1998) 496–517.